

3-D Modeling of Heat Transport in Wendelstein 7-X Startup Plasmas with EMC3-EIRENE

F. Effenberg¹, Y. Feng², O. Schmitz¹, S. A. Bozhenkov², H. Frerichs¹, J. Geiger², H. Hölbe², M. Jakubowski², R. König², M. Krychowiak², H. Niemann², T. Sunn Pedersen², D. Reiter³, L. Stephey⁴, G. A. Wurden⁵ and W7-X Team²

¹Department of Engineering Physics, University of Wisconsin - Madison, WI 53706, USA

²Max-Planck-Institut für Plasma Physik, 17491 Greifswald, Germany

³IEK 4, Forschungszentrum Jülich GmbH, 52425 Jülich, Germany

⁴HSX Plasma Laboratory, University of Wisconsin - Madison, WI 53706, Wisconsin, USA

⁵Los Alamos National Laboratory, PO Box 1663, Los Alamos, NM 87545, USA

Corresponding Author: effenberg@wisc.edu

Abstract:

The magnetic edge topology of the Wendelstein 7-X limiter startup field configuration features separated magnetic flux tubes of three different target to target connection lengths L_C . Simulations are performed with the 3-D plasma edge fluid and kinetic neutral transport Monte Carlo Code EMC3-EIRENE in order to provide a systematic assessment of the governing mechanisms of the 3-D plasma edge heat transport and its relation to the magnetic topology. The standard limiter configuration is compared with a configuration of increased rotational transform ($\nu_{edge} = 0.87 \rightarrow 0.91$). It is shown that the configuration with higher ν_{edge} features a re-distribution of L_C in the boundary. This change of the magnetic topology causes changes in the plasma profiles and the local limiter heat loads. The levels of parallel heat fluxes q_{\parallel} slightly differ dependent on L_C and two different decay regimes are found in the near and far scrape off layer (SOL). The characteristic power e-folding length is found in the near SOL to be $\lambda_{q_{\parallel}} \approx 1.1-1.6$ cm and $\lambda_{q_{\parallel}} \approx 1.8-3$ cm in the far SOL assuming densities of $n_{LCFS} \approx 5.5 \cdot 10^{18} \text{ m}^{-3}$ and heating of $P_{ECRH} = 1-3$ MW for the two rotational transforms considered. First comparisons with IR camera data show a good qualitative agreement with the predicted distributions of the limiter heat loads for both configurations.

1 Introduction

The optimized stellarator Wendelstein 7-X (W7-X) was operated in a limiter configuration [1, 2, 3] during the first plasma operation phase (OP1.1). The standard field configuration during this scenario is chosen such that the main SOL domain consists mostly of closed magnetic surfaces without island structures [1]. Five graphite limiters were installed at the bean shaped symmetric cross sections defining the last closed flux surface (LCFS) and

the SOL. They are designed to prevent high heat and particle loads to unprotected in-vessel components since the graphite divertor target plates were not yet installed. They were positioned to act as main recycling and impurity sources being able to absorb a maximum deposited energy per discharge of 400 kJ each (in total 2 MJ) at maximum heat loads of 10 MWm^{-2} [1]. The limiter shape was chosen based on a field line diffusion method to achieve a uniform heat load distribution and prevent peak loads P_{peak} from exceeding the design limits at an input power of about $P_{in} = 4 \text{ MW}$ [2]. Despite the closed flux surface geometry of the vacuum field, the limiters create, due to their shape and localization, a 3-D helical boundary such that the heat and particle exhaust still remains a 3-D edge transport issue similar to the later island divertor configuration [4, 5]. In some cases limiter field configurations with slightly increased rotational transform ι were applied. Measurements were undertaken to study the impact of a topology change on plasma edge transport and plasma surface interactions (PSI). In this contribution the standard limiter configuration is compared with the configuration featuring the highest ι used in OP1.1 since here the strongest effects due to shifts of resonances and flux surfaces are expected. In the following, an investigation of the parallel heat fluxes q_{\parallel} for W7-X startup scenarios is presented. Like in case of ITER and DEMO [6], investigating, controlling and mitigating the heat loads onto plasma facing components is a crucial topic in 3-D devices like W7-X striving for steady state high performance operation. The fully 3-D fluid plasma edge and kinetic neutral transport Monte Carlo code EMC3-EIRENE [7],[8] is applied as modeling tool. EMC3 solves a set of reduced Braginskii fluid equations for particles, parallel momentum, and energies for electrons and ions. EIRENE solves the kinetic transport equations for neutral atoms and molecules including collisional processes. Based on an initial interpretation of experimental results updated 3-D transport studies were performed using boundary conditions close to the experimentally realized scenarios discussed in section 2. The heat load distribution predicted by EMC3-EIRENE was reported to be correlated to L_C in the standard limiter configuration [3]. Data from IR thermography available now [9] enable first qualitative comparisons with predicted effects from the modeling. The clear decomposition of the magnetic edge topology into separate magnetic flux tubes is used to resolve the dependence of the downstream q_{\parallel} and the resulting deposited target heat loads q_{depo} on the magnetic parallel length scale L_C . These are discussed in section 3. A conclusion is provided in section 4.

2 Topology and boundary conditions of the limiter scenarios

The standard vacuum magnetic field configuration used in OP1.1 features an edge iota value of $\iota_{LCFS} = 0.87$. A complete vacuum Poincaré plot of the bean shaped symmetry cross section is shown in figure 1a. A comparison with figure 1b shows that the limiters cut a boundary domain consisting of closed magnetic flux surfaces. The $\iota = 5/5$ divertor islands are shifted far outside of the limiter radius (not included in the Poincaré plot), while the $\iota = 5/6$ resonances are located within the LCFS close to the limiter. As a

result any (significant) short circuiting within the edge transport region by fast transport around island separatrices is avoided. The domains of different colors in the boundary domain in figure 1b represent the limiter to limiter connection lengths L_C . The magnetic SOL boundary decomposes into three types of helical magnetic flux bundles of different lengths L_C [3]. One identifies $L_C \approx 36$ m, 43 m and 79 m, corresponding to 1.0, 1.2 and 2.2 toroidal windings of open magnetic fieldlines between intersections by a limiter. Longer L_C in the very edge appear only because intersections with in-vessel structures are not taken into account in the modeling.

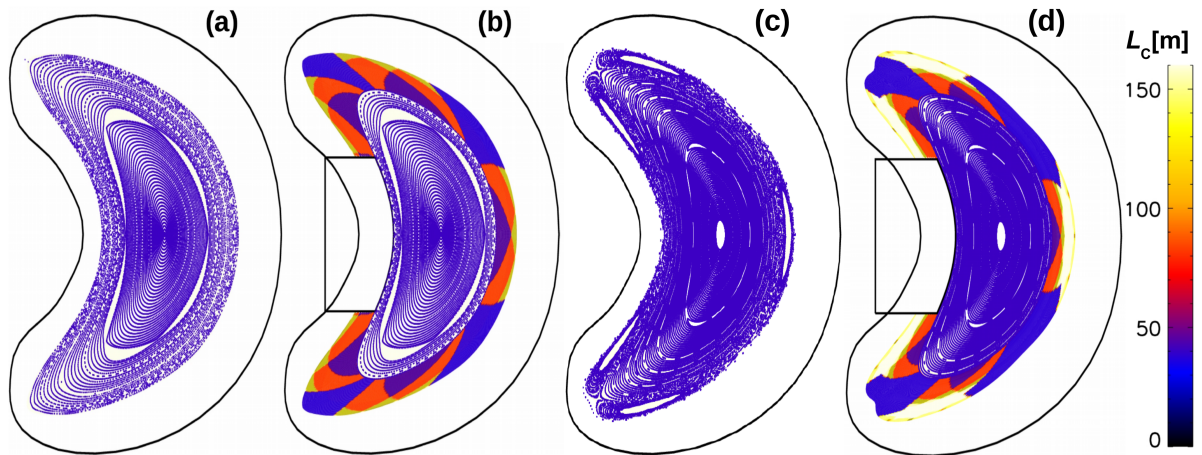


FIG. 1: (a) Poincaré plot of vacuum magnetic field at bean shaped symmetry plane with $\nu_{LCFS} = 0.87$. (b) L_C profile corresponding to open field lines caused by the limiters for $\nu_{LCFS} = 0.87$. (c) Poincaré plot of vacuum magnetic field at bean shaped symmetry plane for $\nu_{LCFS} = 0.91$. (d) L_C profile corresponding to open field lines caused by the limiters for $\nu_{LCFS} = 0.91$.

The second limiter configuration considered in this study was applied at the end of OP1.1 and features an increased rotational transform of $\nu_{LCFS}=0.91$. The complete vacuum Poincaré plot of this increased ν magnetic field scenario is shown in figure 1c. In comparison to the standard limiter magnetic field scenario in figure 1a the 5/5 main resonances are shifted further inwards cutting back the domain of smooth closed magnetic flux surfaces in the outer boundary. Also, the 5/6 resonances are shifted deeper into the confinement domain and reduced in size. The L_C profile for this higher ν scenario is shown in figure 1d. Near the LCFS the SOL features the same three types of magnetic flux tubes like the standard ν case. However, the volume of the shortest flux tube ($L_C \approx 36$ m) is increased at the expense of the remaining ones. In the far edge the profile features domains of long and infinite L_C corresponding to the 5/5 islands and their only partial intersection with the limiters. Within these island domains enhanced radial transport is in principal possible. But they are located several power decay lengths distant from the LCFS and might be limited additionally by in-vessel structures not considered here (e.g. along the top of the limiter one measures between LCFS and island a distance of ≈ 5 cm). Based on the scenarios described above EMC3-EIRENE transport simulations were performed for pure

hydrogen plasmas. Various predictive studies have been performed in the past addressing scans of densities, anomalous transport coefficients and impact of intrinsic and seeded impurities as reported in [3]. In the following boundary conditions for hydrogen plasma close to actual experimental conditions are applied for iteration towards interpretation of experimental results.

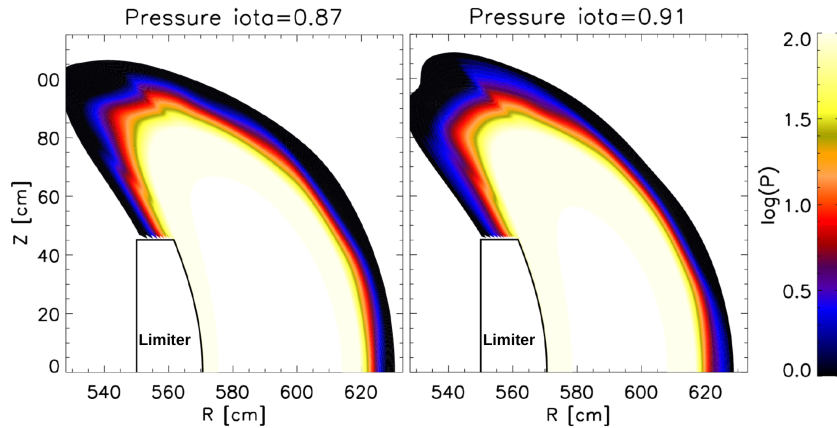


FIG. 2: 2-D logarithmic pressure profiles for $n_{LCFS} \approx 5.5 \cdot 10^{18} \text{ m}^{-3}$, $P_{ECRH} = 1 \text{ MW}$. (Left) Configuration with $\iota_{LCFS} = 0.87$. (Right) Configuration with $\iota_{LCFS} = 0.91$

The density at the LCFS was fixed to $n_{LCFS} \approx 5.5 \cdot 10 \text{ m}^{-3}$. The input power was set in a range of $P_{in} = 1-3 \text{ MW}$, in which electron-cyclotron resonance heating (ECRH) and the heat transfer from electrons to ions mediated by collisions is modeled by setting $P_{in,e^-} = 0.9P_{in}$ and $P_{in,ion} = 0.1P_{in}$. The anomalous cross field coefficients were fixed at $D_{\perp} = 1 \text{ m}^2\text{s}^{-1}$, $\chi_{\perp,e,i} = 3D_{\perp}$. The 2-D plasma pressure profiles ($p = nk_B T$) are shown for $P_{in} = 1 \text{ MW}$ in figure 2 for the standard and increased ι field configurations (left and right). In previous studies it was shown that the SOL plasma parameters are poloidally modulated with L_C [3]. The comparison of the pressure profiles in figure 2 with the L_C profiles in figure 1(left) and figure 1(right) shows that the pressure distribution changes in correlation with the re-distribution of connection lengths during the ι increase. Based on the scenarios considered here, first comparisons with IR camera data and estimation of power width are undertaken in the following.

3 Geometry dependence of power width $\lambda_{q\parallel}$

For the scenarios discussed in the previous section the heat fluxes are calculated with EMC3-EIRENE. In order to investigate how the limiter heat load distribution is related to the magnetic flux tube topology, the deposition of the parallel heat fluxes (q_{depo}) and a mapping of the connection lengths on the limiter surface are calculated for the standard limiter scenario and the higher ι scenario. The L_C distributions are shown in figure 3a as a front view in direction of the minor radius onto the limiter. In both cases the diagonal red stripes correspond to the domain where the long magnetic flux tubes (79 m) connect to the limiters. The remaining surface area connects to the transport channels of short

L_C (36 m, 43 m). The resulting 2-D distributions of the heat loads for both scenarios are shown in figure 3c and compared with the IR thermography measurement [9] in figure 3b. The numerically predicted change of the limiter heat loads in correlation with L_C is clearly shown by comparison of figure 3a and figure 3c. The comparison of these numerical results with the IR thermography results for the surface temperature distributions in figure 3b shows a good qualitative matching between predictions and experiment. Further interpretation of the limiter PSI and heat load measurements by 3-D modeling is in progress [10, 11, 12].

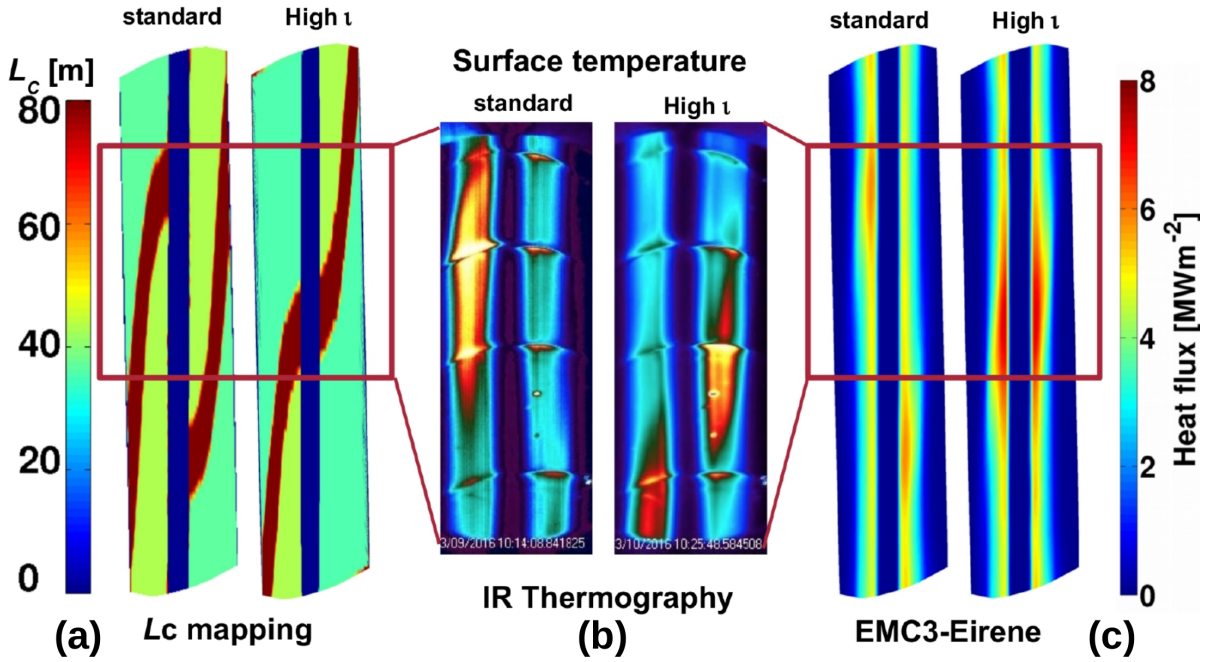


FIG. 3: Comparison of EMC3-EIRENE calculations with IR tomography. The red frames represent the observation domain covered by the camera view. (a) Mapping of the target to target connection lengths L_C onto the limiters for $\nu_{LCFS}=0.87$ (left) and $\nu_{LCFS}=0.91$ configuration (right). (b) Front view of limiters by IR tomography. The colored patterns represent the surface temperature. Left: $\nu_{LCFS}=0.87$, right: $\nu_{LCFS}=0.91$ (c) Calculated limiter heat loads with EMC3-EIRENE for $\nu_{LCFS}=0.87$ (left) and $\nu_{LCFS}=0.91$ (right).

In figure 4(left) a scan of the deposited heat load (q_{depo}) at a height of $Z = -0.2$ m along the limiter surface (s goes in toroidal direction) is shown for low and high ECR heating for standard (blue and red) and increased ν (green and cyan). The maximum deposited peak loads are for $P_{in} = 3$ MW at $q_{depo,max}(Z = -0.2m) = 8-9$ MWm^{-2} and drop to 2-2.5 MWm^{-2} for $P_{in} = 1$ MW. Defining a radial coordinate r_{eff} based on the flux surfaces within the boundary the radial downstream heat flux profiles averaged over each L_C domain separately can be represented as shown in figure 4(center). The solid line represents the radial decay within the long connection lengths flux tube while the dashed and dotted lines represent the heat flux within the short L_C domain. The faster parallel losses along short L_C cause a stronger decay compared to long L_C . In the far SOL the temperature

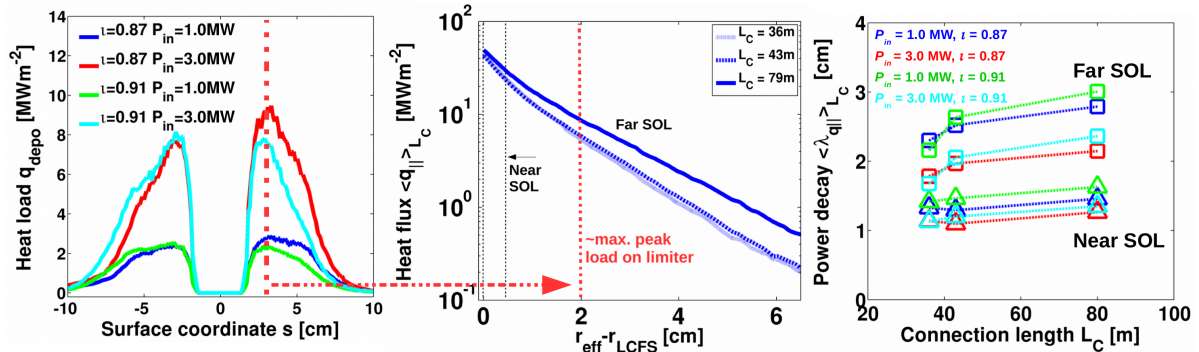


FIG. 4: (Left) Local heat loads on the limiter surface at $Z = -0.2\text{m}$ calculated with EMC3-EIRENE. (Center) Heat flux profiles $q_{\parallel}(L_C)$ (averaged over L_C domain). (Right) Inferred near and far SOL power decays $\lambda_q(L_C)$.

drop leads to a reduction of the parallel loss rate and therefore a flattening of λ_q compared to the steeper near SOL decay. By fitting near and far SOL power decay for the different flux tubes one obtains a dependence as shown in figure 4(right). For both scenarios the power width increases with reduction of P_{in} . The power decay λ_q differs by a factor 2-3 between near and far SOL. However, for the density and power scenario considered here the dependence of λ_q is less effective in the near SOL compared to the decay in the far SOL. The topology dependence is stronger in the far SOL for higher heating power. Due to the less effective geometry function at the limiter heat load tail the far SOL λ_q is easier to access experimentally. The vertical red dashed lines in figures 4(left and center) identify for the standard ι case the position of the limiter peak heat load in the flux surface averaged heat flux profiles.

4 Summary

A first comparison of 3-D modeling of heat fluxes for two different limiter configurations is presented. It is shown that the higher ι configuration features the same three types of helical magnetic flux tubes in the SOL. The connection lengths distribution causes different magnetic footprints on the limiters for the increased ι configuration and a change in the poloidal plasma pressure distribution. A first comparison of the deposited heat fluxes with experimental IR thermography shows for both configurations good qualitative agreement with the predictions from 3-D modeling. The analysis of q_{\parallel} reveals a different decay behavior in the near and far SOL and a weak dependence on L_C for $n_{LCFS} = 5.5 \cdot 10^{18} \text{ m}^{-3}$. The experimentally accessible far SOL power decay features a stronger dependence on L_C . A mitigation of peak fluxes and broadening of $\lambda_{q_{\parallel}}$ can be achieved by reducing power entering the SOL. The power reduction in the scenario addressed can be interpreted as a proxy of power losses within the confinement domain due to impurities or charge exchange neutrals.

5 Acknowledgements

This work was supported in part by the U.S. Department of Energy (DoE) under grant DE-SC0014210 and by start up funds of the Department of Engineering Physics and of the College of Nuclear Engineering at the University of Wisconsin - Madison, USA. This research was performed using the computer resources and assistance of the UW-Madison Center For High Throughput Computing (CHTC). This work has been carried out within the framework of the EUROfusion Consortium and has received funding from the Euratom research and training programme 2014-2018 under grant agreement No 633053. The views and opinions expressed herein do not necessarily reflect those of the European Commission.

References

- [1] T. Sunn Pedersen et al., “Plans for the first plasma operation of Wendelstein 7-X”, *Nuclear Fusion*, 50(12):126001, 2015.
- [2] S. A. Bozhenkov, F. Effenberg, et al., “Limiter for the early operation phase of W7-X” *41st EPS Conference on Plasma Physics*, P1.080, Berlin (2014)
- [3] F. Effenberg, Y. Feng, et al., “Numerical investigation of plasma edge transport and limiter heat fluxes in Wendelstein 7-X startup plasmas with EMC3-EIRENE” *submitted for publication in Nuclear Fusion 2016*
- [4] D. Sharma, Y. Feng, F. Sardei, “A 3D Monte-Carlo study of the W7-X island divertor transport for different magnetic configurations” *Nuclear Fusion*, 46:S127–S138, 2006.
- [5] Y. Feng, et al., “EMC3/EIRENE Transport Modelling of the Island Divertor in W7-X” *35th European Physical Society Conference on Plasma Physics and 10th International Workshop on Fast Ignition of Fusion Targets. Contributed Papers*, volume 32D of ECA, Hersonissos, Crete, 2008. European Physical Society.
- [6] T. Eich et al., “Inter-ELM Power Decay Length for JET and ASDEX Upgrade: Measurement and Comparison with Heuristic Drift-Based Model” *Phys. Rev. Lett.*, 107:215001, 2011.
- [7] Y. Feng, F. Sardei, and J. Kisslinger, “3D Fluid Modelling of the Edge Plasma by Means of a Monte Carlo Technique” *Journal of Nuclear Materials*, 266-269:812818, 1999.
- [8] D. Reiter, “Randschicht-Konfiguration von Tokamaks: Entwicklung und Anwendung stochastischer Modelle zur Beschreibung des Neutralgastransports” *Technical Report Jül-1947*, 1984.
- [9] G. A. Wurden, L. Stephey, et al., “A high resolution IR/visible imaging system for the W7-X limiter” *Review of Scientific Instruments*, 87(11), 2016.
- [10] H. Niemann, M. Jakubowski, et al., “Power loads in the limiter phase of Wendelstein 7-X” *43rd EPS Conference on Plasma Physics*, P4.005, Leuven (2016)
- [11] L. Stephey, G. A. Wurden, et al., “Spectroscopic imaging of limiter heat and particle fluxes and the resulting impurity sources during Wendelstein 7-X startup plasmas” *Review of Scientific Instruments*, 87, 11D606 (2016)
- [12] H. Frerichs, F. Effenberg, et al., “Synthetic plasma edge diagnostics for EMC3-EIRENE, highlighted for Wendelstein 7-X” *Review of Scientific Instruments*, 87, 11D441 (2016)